applied optics

Investigation of impact and spreading of molten nanosized gold droplets on solid surfaces

Daozhi Shen,[1] Guisheng Zou,[1] Lei Liu,[1,*] Aiping Wu,[1] Walter W. Duley,[2] and Y. Norman Zhou[3]

[1]Department of Mechanical Engineering, The State Key Laboratory of Tribology, Tsinghua University, Beijing 100084, China
[2]Department of Physics and Astronomy, University of Waterloo, Waterloo N2L 3G1, Canada
[3]Department of Mechanical & Mechatronics Engineering, University of Waterloo, Waterloo N2L 3G1, Canada
*Corresponding author: liulei@tsinghua.edu.cn

Received 3 January 2018; revised 7 February 2018; accepted 9 February 2018; posted 13 February 2018 (Doc. ID 318713); published 14 March 2018

Understanding the impact dynamics and spreading of molten nanosized droplets on a solid surface is a crucial step towards the design and control of nano-fabrication in many novel applications of nanotechnology. In this context, molecular dynamic (MD) simulations have been conducted to compute temperature and dynamic contact angles of nano-droplets during impact. The evolution of the morphology of a molten metallic nano-droplet impacting on a substrate has been studied using a combination of experimental and simulation techniques. Femtosecond lasers have been used to transfer nanosized gold droplets. Droplet morphology calculated in MD simulations is found to be in good agreement with that seen in scanning electron microscopy (SEM) images. It is found that the spreading of nanoscale molten gold droplets upon impact is enhanced by increasing the droplet impact energy. As observed in experimental data, MD simulation results show that a high droplet-substrate heat transfer rate together with increased wettability of the substrate facilitates spreading and results in a thinner metal deposit after solidification.

OCIS codes: (350.3450) Laser-induced chemistry; (020.2070) Effects of collisions; (160.4236) Nanomaterials; (160.3900) Metals; (350.3390) Laser materials processing; (310.1860) Deposition and fabrication.

https://doi.org/10.1364/AO.57.002080

1. INTRODUCTION

Spreading of a high-speed droplet impacting on a dry solid surface is common in nature and is an important phenomenon in many scientific and technological processes. With the development of nanotechnology, the impingement of nanosized droplets on surfaces plays an important role in many novel applications including micro/nano additive manufacturing, [1–3] silicon photonics, [4–7], particle-based sensors [8], and pulsed laser deposition [9,10]. For example, laser jetting of molten nano-droplets on a substrate has been recently investigated in an application involving the micro-manufacture of 3D printed structures [3]. The impact and spreading of molten nano-droplets on a substrate is known to have a significant effect on droplet adhesion [2]. This effect is also important in the laser-induced transfer of periodic arrays of gold nano-droplets on silicon substrates for optoelectronic applications [8]. The performance of optoelectronic devices is largely determined by the final shape of deposited nanoparticles, and is determined by the impact and spreading of molten nano-droplets as they hit the substrate. However, a detailed analysis of the dynamic properties of molten metal nano-droplets impacting on a dry solid surface has not yet been carried out.

The dynamic behavior of a droplet impacting on a solid substrate at room temperature is a result of many interacting physical effects. Important factors include droplet momentum [11], the contact angle [12,13], ambient pressure [14,15] and the roughness of the solid substrate [16]. For example, Riboux and Gordillo have outlined a model of the critical impact speed for splashing [11]. Xu *et al.* found that splashing can be completely suppressed by decreasing the ambient pressure [15] while Latka *et al.* reported that surface roughness inhibits the formation of thin sheets even though it also increases prompt splashing [16]. The impact and spreading of a high-temperature molten droplet on a cold solid substrate is also affected by heat transfer between the molten droplet and the surface [17,18], making the physical process very complex. As a result, most previous studies have focused on the impact dynamics of molten droplets with sizes >10 μm because it is easier to control the above parameters during the experiment. We have recently reported the impact and splashing behavior of submicron gold droplets on solid surfaces and showed that the droplet-substrate heat transfer rate is a key factor in the overall process [17]. Only numerical simulations were used to study the impact dynamics of nano-droplets at room temperature

since little experimental data is available because of difficulties in the generation and observation during impact of high-speed, high-temperature, molten nanosized droplets [19–22]. Due to these limitations, we have little knowledge on the dynamics of molten nanosized droplets impacting on dry solid substrates.

In this study, we use a femtosecond (fs)-laser-induced forward transfer (fsLIFT) technique to generate high-speed nanosized gold droplets having high internal temperature to facilitate the study of droplet impact on gold and silicon substrates. The gold substrate has a higher heat transfer rate and better wettability than that of silicon when gold droplet contacts the substrate. This difference enables a straightforward comparison of the effect of physical parameters in the experiment. Molecular dynamic (MD) simulations have been carried out to explore detailed impact behavior and also to obtain the temperature and contact angle of gold droplets on these substrates during the impact and spreading process. Direct observation of droplet morphology after solidification confirms the results of MD simulations.

2. METHODOLOGY

A. Experimental Procedure

In these experiments, femtosecond laser pulse irradiation of a 10 nm thick layer gold film coated by magnetron sputtering on a 320 μm thick glass plate generates molten nanosized gold droplets. The detailed schematic of this fsLIFT system can be found in our previous paper [17]. To obtain gold droplets having a diameter of ∼80 nm, single fs laser pulses with an energy of ∼100 nJ were focused using a microscope objective (Olympus) with ×100 magnification and a numerical aperture (NA) of 0.9 through the glass onto the thin gold donor film. The substrate that received the droplets was placed at distances of 120, 240, and >500 μm from the gold donor film. Distance was varied to obtain different total droplet impact energy on the substrate. All operations were carried out in air at atmospheric pressure. The experimental setup is shown in Fig. 1(a).

In order to investigate how heat transfer rate and wettability between the droplet and substrate affect the impact results, two different types of substrates were used as the receptors for transferred metal: (1) single crystal silicon with a thickness of 500 μm and (2) a 50 nm gold film coating on a silicon wafer with a 5 nm chromium adhesion layer. The substrates were immersed into a mixed solution of acetone and ethanol under ultrasonic for 20 min and were dried by blowing compressed air. Then the substrates were cleaned by plasma for 5 min to remove the possible surface contaminations. Thereafter the experiment of nanosized gold droplet transfer was conducted immediately. X-ray photoelectron spectroscopy (XPS) and an ellipsometer were used to characterize the surface of silicon substrates. We use scanning electron microscopy (SEM) (ZEISS Inc.) images to analyze the morphology of solidified nanosized gold droplets after deposition on these two substrates.

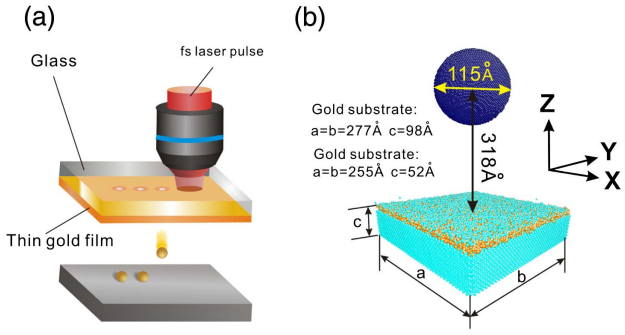

Fig. 1. (a) Schematic of the femtosecond laser forward transfer (fsLIFT) for the generation of nanosized gold droplets. (b) Schematic plot of initial sate in simulation system. There are 46,894 atoms in the gold droplet, 449,198 atoms in the gold substrate, and 187,976 atoms in the silicon substrate. There is a surface amorphous SiO_2 layer with a thickness of 12 Å in silicon substrate.

B. Simulation Method

MD simulations were carried out to investigate the impact and spreading of nanosized gold droplets on gold and silicon substrates. The interaction between gold atoms was modelled with an embedded atom method (EAM) potential. The total energy of a system of gold atoms is then [23]

$$E = \sum_i \left(F_i(\rho_i) + \frac{1}{2} \sum_{j \neq i} \phi(r_{ij}) \right), \tag{1}$$

where $F_i(\rho_i)$ is the energy required to embed an atom i in a uniform electron gas of density ρ_i, and $\phi(r_{ij})$ is the pairwise interaction of atoms i and j separated by the distance r_{ij}. As the pure single crystal silicon is easily oxidized when placed in air, there is a thin layer of amorphous silicon dioxide (SiO_2) with thickness of ∼2 nm on the surface of silicon substrate (measured by ellipsometer). To mimic this experimental condition, a thin amorphous silicon dioxide layer was added on the top of silicon substrate in the computing system for the simulation of impact and spreading of gold droplets on silicon substrate. For interactions between silicon atoms and interactions between silicon and oxygen atoms, we choose a Tersoff potential because of its flexibility, the short range of the interatomic interactions, and its success in a wide range of applications in condensed phases [24]. The interatomic potential in a silicon atom system is described elsewhere [25,26]. In modelling the gold droplet impact on the silicon substrate, the interactions between gold and silicon atoms are given by the Lennard–Jones (LJ) potential [27],

$$E_{\text{Au-Si}} = 4\varepsilon_{\text{Au-Si}} \left[\left(\frac{\sigma_{\text{Au-Si}}}{r} \right)^{12} - \left(\frac{\sigma_{\text{Au-Si}}}{r} \right)^{6} \right], \tag{2}$$

where $\sigma_{\text{Au-Si}}$ and $\varepsilon_{\text{Au-Si}}$ are the characteristic length and energy parameters of the LJ potential, respectively, and r is the distance between gold and silicon atoms. To comply with common practice and to ensure transferability of all aspects of the force field, we use the Lorentz–Berthelot mixing rules for the LJ parameters [28], $\sigma_{\text{Au-Si}}$ and $\varepsilon_{\text{Au-Si}}$,

$$\sigma_{\text{Au-Si}} = \frac{\sigma_{\text{Au-Au}} + \sigma_{\text{Si-Si}}}{2}, \tag{3}$$

$$\varepsilon_{\text{Au-Si}} = \sqrt{\varepsilon_{\text{Au-Au}} \varepsilon_{\text{Si-Si}}}, \tag{4}$$

with $\sigma_{\text{Au-Au}} = 2.934$ Å, $\varepsilon_{\text{Au-Au}} = 0.00169$ eV (from Ref. [29]), $\sigma_{\text{Si-Si}} = 2.0951$ Å, and $\varepsilon_{\text{Si-Si}} = 2.1683$ eV (from Ref. [30]). From Eqs. (3) and (4), $\sigma_{\text{Au-Si}} = 2.51455$ Å and $\varepsilon_{\text{Au-Si}} = 0.06032$ eV. The cutoff radius was set as 7 Å.

The LJ potential is also used to describe the interactions between gold and oxygen atoms. $\sigma_{\text{Au-O}}$ and $\varepsilon_{\text{Au-O}}$ are calculated as 0.0034 eV and 3.027 Å from the above equations, respectively.

The large-scale atomic/molecular massively parallel simulator (LAMMPS) molecular dynamic code [31] was used to carry out computer simulation of the ensemble. The computational system consists of a simulation box with dimensions of 628 Å in the X and Y directions and 820 Å in the Z direction and with periodic boundary conditions in all directions. The time step was 2 fs in all simulations. Figure 1 shows the geometry for a 115 Å diameter gold particle above a substrate with dimensions of 277 Å × 277 Å × 98 Å (gold) or 250 Å × 250 Å × 52 Å (silicon substrate). There is a surface amorphous SiO_2 layer having a thickness of 12 Å in silicon substrate. The size of gold particle in this model is in the same scale compared to the gold nanodroplet generated using fsLIFT in the experiment. The initial distance between the center of the droplet and the surface is 318 Å. Overall, there are 46,894 atoms in the gold droplet, 449,198 atoms in the gold substrate, and 187,976 atoms in the silicon substrate. During simulation, atoms in the lowest layer of the substrate are fixed in position. This layer has a thickness of 25 Å in the gold substrate and 10 Å in the silicon substrate. The dimension of droplet and substrate is shown in Fig. 1(b).

The simulation consists of two stages. In the initial stage, a gold nano-cluster with a face centered cubic (FCC) lattice is placed in the initial position and the linear and angular momenta of the gold droplet are zeroed every 2 fs step. This prevents movement of the droplet. Following this, the gold nano-cluster and the substrate are equilibrated at 2.5 K in 8000 steps using an NVT ensemble by a Nose–Hoover thermostat [32]. After that, the gold nano-cluster is heated to 1500 K and the substrate is heated to 300 K in 28,000 steps and kept at that temperature for 2000 steps to allow equilibration. After equilibration, restrictions on the linear and angular momenta of the gold droplet are removed. At this point in time, all atoms in the gold droplet are given an additional momentum in the Z direction, which marks the beginning of the second stage. In this stage, velocities of 100, 200, 300, or 400 m/s are assigned to the gold droplet and the Nose–Hoover thermostat is removed from the simulation domain. The NVT ensemble is replaced by an NVE ensemble that updates the positions and velocities of the atoms. These settings permit atoms to interact more closely, providing a better simulation of experimental conditions. During this process, energy is allowed to be transferred among atoms subject to conservation of the overall system energy. In order to model the full development of the impact and spreading of gold droplet process on substrates, this stage runs for 500 ps. The translation energy is excluded from droplets when calculating the temperatures. To investigate the role played by heat transfer to the substrate during spreading, the lattice temperature of the droplet can be lowered by selectively removing energy from the lattice at a rate ΔH eV/ps and adding into the atoms in substrate. In each time increment, the calculation follows two dynamic processes. First, the velocity of each atom in droplet and substrate is reduced and increased, respectively. But the velocity of the center of the mass is maintained. The velocity and coordinates of each atom are then updated in an exchange of atomic momenta required by the NVE ensemble settings. This method has the effect of reducing the droplet temperature while conserving momentum. Adjusting the value of ΔH permits a comparison of spreading on surfaces having different wettability while maintaining constant thermal conductivity.

3. RESULTS AND DISCUSSION

Figure 2 shows the contact angles of water drops on those substrates. The gold and silicon substrates become very hydrophilic after treated by plasma, indicating that the cleanliness of the surfaces of the substrates is largely improved. Although the plasma-treated substrates exhibit good wettability, the contact angle of water on gold substrate is still visible, which should be attributed to the inevitable slight contaminations on the substrate surfaces when exposed in air. Aerodynamic drag and convective cooling decrease droplet velocity and droplet internal temperature prior to impact on the receptor substrate. As noted above, the total energy prior to droplet impact decreases with an increase in the distance z between the donor and receiver substrates [17]. Figures 3(a)–3(c) show the effect of different flight distances on the impact of a molten 80 nm diameter gold droplet on a gold substrate. At high-impact energy [$z = 120$ μm, as shown in Fig. 3(a)], the molten droplet spreads uniformly to form a thin disk-like splat structure with a thicker smooth peripheral rim. At intermediate impact energy [$z = 240$ μm, as shown in Fig. 3(b)], the droplet spreads slightly, forming a spherical cap with a very smooth periphery. At low impact energy [$z > 500$ μm, as shown in Fig. 3(c)],

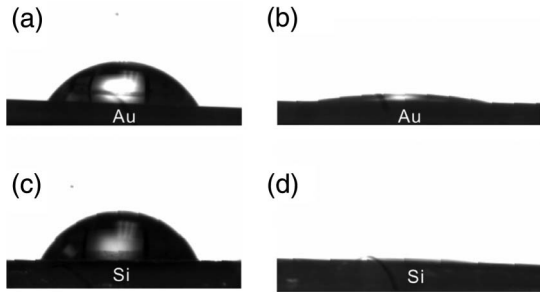

Fig. 2. Contact angles of water drop on (a), (b) gold substrates and (c), (d) silicon substrates. Surface status is (a), (c) without plasma treatment and (b), (d) after plasma treatment.

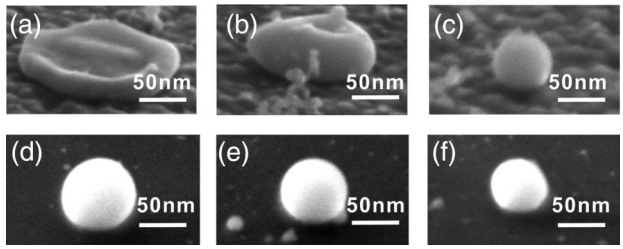

Fig. 3. Images of gold droplets (~80 nm in diameter) after impact and solidification on the surface of (a)–(c) gold and (d)–(f) silicon substrates. Flight distances are: (a), (d) 120 μm, (b), (e) 240 μm, and (c), (f) >500 μm. All images are taken at an angle of 75°.

the droplet remains spherical after contact as droplet solidification is rapid, inhibiting spreading. Although the droplet temperature decreases with the flight distance, these results indicate that the nanosized gold droplet was still liquid after a traveling distance of 240 μm.

Figures 3(d)–3(f) show the morphology of gold droplets following impact and solidification on a silicon surface. The gold droplets are seen to be spherical after impact at all flight distances, unlike the results obtained for impact on a gold substrate.

These results clearly show that the physical properties of the substrate have a strong effect on the impact and spreading process for molten nanosized gold droplets. To investigate this effect, MD simulations can be used to reveal details of the interaction mechanism. Figure 4 traces the effect of different impact velocities on the impact and spreading of a molten 11.5 nm diameter gold droplet on a gold substrate. As shown in Fig. 4(a), following contact on the gold surface at an impact velocity of 400 m/s ($t = 66$ ps), the droplet rapidly adopts a cap-like morphology ($t = 72$ ps). A precursor film then develops in front of the droplet ($t = 80$ ps), extending to a maximum diameter at $t = 108$ ps. This morphology is conserved until the droplet solidifies into a metal disk ($t = 174$ ps). A similar spreading sequence is observed at an impact velocity of $v = 200$ m/s, but the resulting solidified gold disk is thicker [Fig. 4(b)]. After impact at 100 m/s, the droplet solidifies to form a spherical gold cap [Fig. 4(c)].

Figure 5 shows the morphology of an 11.5 nm diameter gold droplet during impact and spreading on a silicon substrate. The droplet contacts the silicon surface at $t = 66$ ps at an impact velocity of 400 m/s and forms a metal cap by $t = 76$ ps. A precursor film develops in front of the droplet and extends to a maximum diameter by $t = 122$ ps. This film

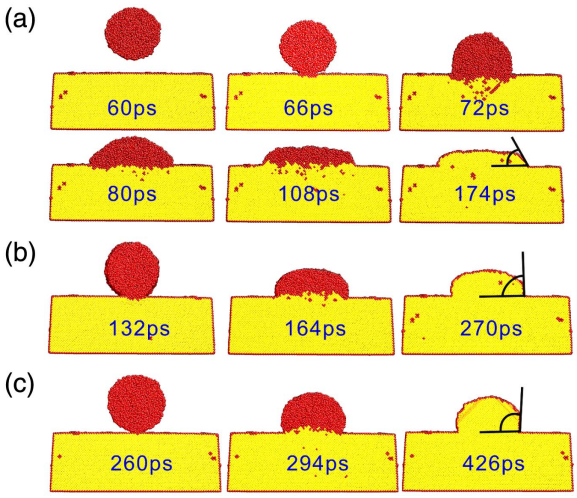

Fig. 4. Snapshots (cross-sectional view) of a gold droplet during impact on a gold substrate surface as calculated from the MD simulation. Time is measured from the initial position of the droplet during flight. The impact velocities are: (a) 400 m/s, (b) 200 m/s, and (c) 100 m/s. The droplet first contacts the substrate at (a) 66 ps (b) 132 ps, and (c) 260 ps. The maximum diameter occurs at (a) 108 ps, (b) 164 ps and (c) 294 ps. The final frame in (a), (b), and (c) corresponds to an image of the droplet after solidification, where yellow indicates that the atoms are present in an FCC structure.

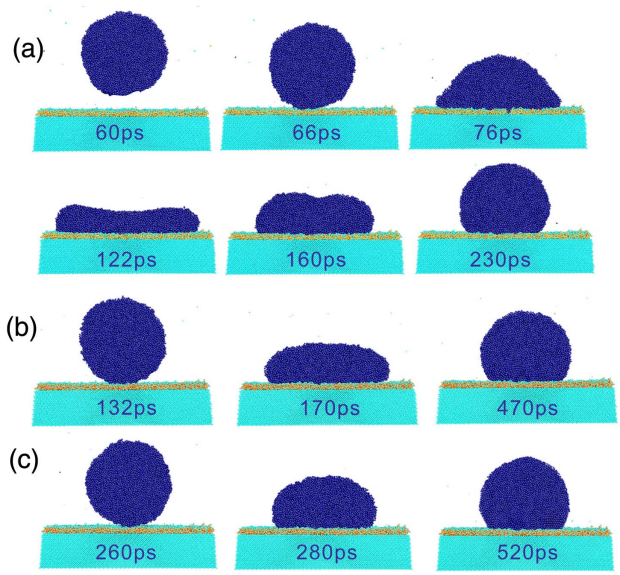

Fig. 5. Snapshots (cross-sectional view) of a gold droplet during impact on a silicon substrate surface as calculated from the MD simulation. Time is measured from the initial position of the droplet during flight. The impact velocities are: (a) 400 m/s, (b) 200 m/s, and (c) 100 m/s. The droplet first contacts the substrate at (a) 66 ps, (b) 132 ps and (c) 260 ps. The maximum diameter occurs at (a) 120 ps, (b) 160 ps and (c) 276 ps. The final frame in (a), (b), and (c) corresponds to an image of the droplet after solidification. Gold atoms are indicated in blue, while silicon and oxygen atoms are green and brown, respectively.

remains liquid and gradually contracts to form a higher metal cap by $t = 160$ ps. This structure becomes spherical after solidification ($t = 230$ ps). Spherical morphology is also observed after solidification at impact velocities of $v = 200$ m/s and 100 m/s [Figs. 5(b) and 5(c)]. The spreading process at lower impact velocity is similar to that seen in Fig. 5(a), except that the precursor film has a smaller maximum diameter.

A comparison between computational simulations and the experimental measurements shows many similarities between predicted and observed morphologies of the final solidified structures after impact and spreading of a gold droplet on the substrates. When the droplet impacts on a gold substrate, both simulation and experiment show that the solidified metal changes from a thin disk to a spherical cap as the impact energy is reduced. When impact occurs on a silicon substrate, the solidified metal remains spherical at all impact energies. These similarities indicate that our MD simulation method provides an accurate representation of the impact and spreading behavior of gold droplets on the two different substrates.

Figure 6 shows the time-dependent internal temperature of gold droplets, calculated at different impact velocities, as they contact and subsequently spread on gold and silicon substrates. As expected, droplet temperature is constant before the droplet contacts the substrate. However, the droplet temperature spikes after the droplet impinges on the gold or silicon substrate at velocities of 400 and 300 m/s. This occurs as the high translational kinetic energy is converted to heat in the droplet. Following this spike, heat transfer between the

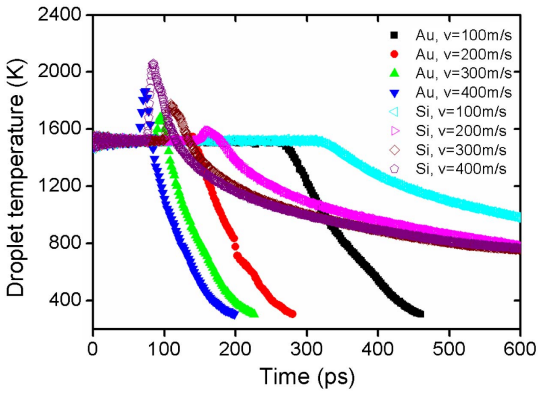

Fig. 6. MD calculation of the internal temperature of a gold nano-droplet with diameter of 11.5 nm during impact on gold and silicon substrate surfaces with different velocities. Translation energy is excluded from system when temperature was calculated. Time is measured from the initial position of the droplets during flight.

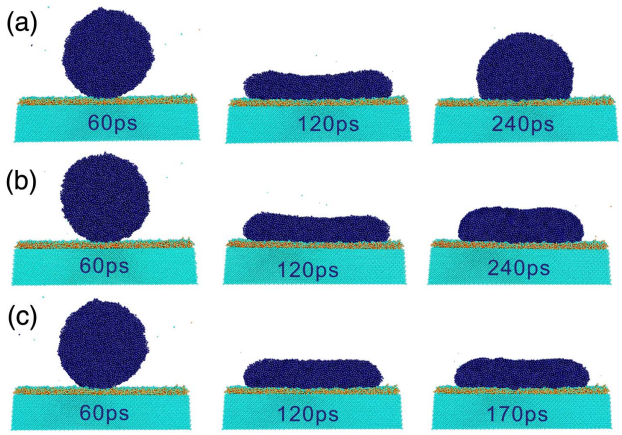

Fig. 7. Snapshots (cross-sectional view) of a gold nano-droplet during impact on a silicon substrate with velocity of 400 m/s as calculated from the MD simulation after different heat subtraction rates from the droplet during impact. Heat subtraction rates are: (a) 10 eV/ps, (b) 100 eV/ps, and (c) 200 eV/ps. Heat subtraction simulates the effect of increasing thermal conduction to the surface. Gold atoms are indicated in blue, while silicon and oxygen atoms are green and brown, respectively. The left image in each sequence represents the initial contact between the droplet and the substrate. The middle image shows the droplet at the moment when the droplet has spread to its maximum diameter, while the right image is a view of the nano-droplet after solidification. Time is measured from the initial position of droplets during flight.

high-temperature droplet and the cold substrate leads to a rapid decrease in internal temperature as shown in Fig. 6. The rapid decline in droplet temperature during cooling on the gold substrate relative to that on silicon is indicative of the role played by thermal conductivity.

The above results clearly show that heat transfer to the substrate is a dominant effect in the spreading and solidification of molten gold nano-droplets. This effect can be investigated in the MD by subtracting heat from the atoms in the gold droplet during spreading on the substrate. This simulates a decrease in droplet temperature without changing wetting conditions. Figure 7 shows the calculated droplet morphology during spreading on silicon after different heat subtraction rates. The impact velocity was set at 400 m/s. At a low heat subtraction rate ($\Delta H = 10$ eV/ps), the gold droplet gradually flows as a thin disk and reaches its maximum area at $t = 120$ ps. Subsequently, the precursor film remains liquid and gradually contracts to form a metal cap. This shape is maintained on solidification [Fig. 7(a)]. The overall process is the same as that which occurs after impact on silicon without additional heat subtraction [see Figs. 5(a) and 7(a)]. At a higher heat subtraction rate ($\Delta H = 100$ eV/ps and 200 eV/ps, as shown in Figs. 7(b) and 7(c), respectively), after reaching a maximum area, the droplet rapidly solidifies, forming a flattened disk-like structure instead of a spherical cluster. At a heat subtraction rate of 200 eV/ps, the droplet spreading process on silicon is similar to that seen on a gold substrate. Despite this similarity, the maximum droplet area during spreading on silicon is much less than on gold, and the solidified disk-like metal structure is thicker on silicon (186 nm^2 and 28 Å for area and thickness, respectively) than that on a gold substrate (143 nm^2 and 43 Å for area and thickness, respectively).

The time-dependent internal temperature and contact angle of a droplet during impact and spreading on a silicon substrate are shown in Figs. 8(a) and 8(b), respectively. It can be seen that the rate of decrease in droplet temperature is enhanced as the heat subtraction rate increases from 10 eV/ps to 200 eV/ps. The cooling rate of a droplet on silicon is greatest when $\Delta H = 200$ eV/ps and is then equivalent to that occurring on a gold substrate. The contact angle of a droplet impacting on a gold substrate rapidly changes from 180° just after collision to 60°. This angle is still a little large and then remains constant until final solidification. Figure 4 shows that the final contact angle is influenced by the impact velocities, which affect the dynamics of spreading of liquid precursor. The very efficient cooling rate of gold substrate may result in fast solidification of the droplet, which inhibits its precursor developing into an equilibrium morphology with a small contact angle. Other factors such as temperature, pressure, and the accuracy of potential chosen in the simulation may also affect the contact angles obtained, which needs further investigation in the future. For impact on silicon, the contact angle also changes from 180° immediately following the collision to 90°. It then rapidly increases to ~110° and maintains this angle until solidification is complete. The final contact angle of a gold droplet on silicon as calculated in our MD simulation is similar to that obtained in other studies, suggesting that de-wetting occurs under these conditions [33,34].

The MD simulations are also in good agreement with SEM images of gold nano-droplets after impact and solidification on gold and silicon substrates. This suggests that the MD simulations also provide a good representation of droplet morphology at and after impact. This agreement, together with the correct prediction of contact angle, shows that the current MD model is a useful methodology for revealing the dynamics of molten gold nano-droplets during impact and spreading on solid surfaces.

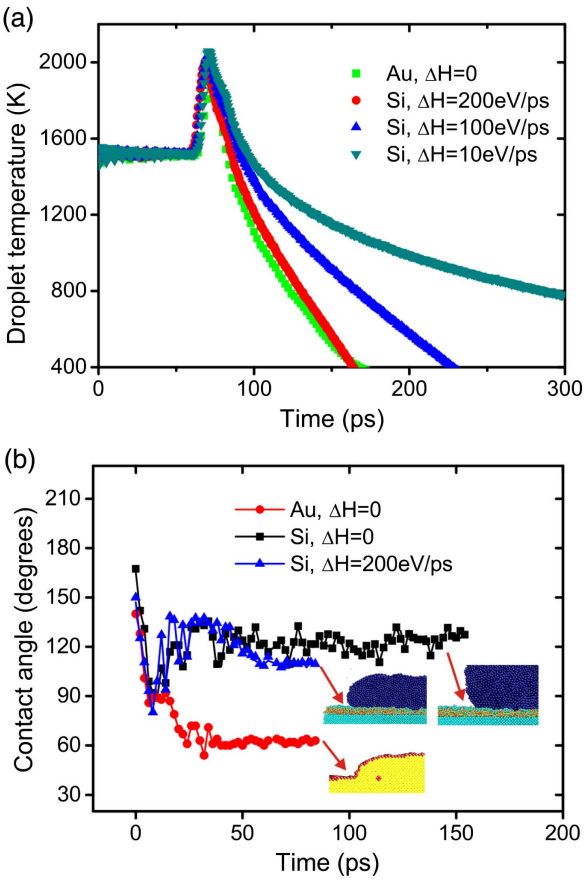

Fig. 8. (a) Calculated internal temperature and (b) contact angle for gold nano-droplets with diameter of 11.5 nm during impact with a velocity of 400 m/s on gold and silicon surfaces incorporating different heat subtraction rates. Translation energy is excluded from system when temperature was calculated. The insets in (b) show a final cross-sectional view of the droplets after solidification. Time is measured from (a) the initial position of the droplet during flight and (b) the moment of droplet contact with the gold or silicon surface.

We have previously reported that heat transfer between a molten sub-micron droplet and a solid substrate is the primary factor controlling the dynamics of the splashing process [17]. The present theoretical and experimental results indicate that heat transfer also plays a key role in spreading and the subsequent solidification morphology of molten nano-droplets on a solid surface. When a molten nano-droplet undergoes a high-speed impact with a substrate, the droplet first spreads radially, forming a large disk. When the heat transfer rate to the substrate is high, this disk or cap-like structure solidifies as shown in Figs. 4(a) and 7(c). A smaller heat-transfer rate allows the original disk to contract, forming a quasi-spherical cluster after solidification. This effect can be clearly seen in Fig. 7, where the cooling rate is varied without altering the wettability of the substrate.

The wettability of the substrate surface is nevertheless an important parameter when a molten nano-droplet undergoes high-speed impact with the surface [35]. However, the substrates for the impact of molten sub-micron droplet have been not cleaned by plasma [17], a process that would reduce the possible contaminations and increase the wettability of solid surfaces, as shown in Fig. 2. To accurately investigate the influence of wetting properties of substrates on the splashing or impact behaviors of sub-micron/nanosized molten droplets, a cleaning process such as plasma treatment for solid substrates is needed to minimize the influence of the surface contaminations. For impact on a non-wetting substrate surface, the high surface tension of the liquid metal inhibits the extension and spreading of the droplet on the substrate. This results in a smaller area of the disk on the surface. A comparison of the simulated spreading of droplets on substrates having different wettability, while maintaining a constant cooling rate, suggests that spreading of the droplet is greatest on the surface with high wettability [see Figs. 4(a) and 7(c)].

In our experiments, the heat transfer rate for gold–gold contact is much higher than that at the gold–silicon interface. In addition, gold has higher wettability than silicon for a molten gold droplet. Our results show that good wettability and a high heat transfer rate promote the formation of disk-like or cap structures from gold nano-droplets impacting on a gold substrate after solidification.

4. CONCLUSION

We have developed a new methodology that combines fs-laser-induced forward transfer (fsLIFT) and molecular dynamic (MD) simulations to trace dynamical processes during the high-speed impact and spreading of molten nano-droplets on gold and silicon solid surfaces. Our analysis is directed toward a determination of the primary factors that control the spreading and solidification of molten gold nano-droplets on these surfaces. MD simulations of these effects are in good agreement with measured data. Both simulation and experiment suggest that high-impact energy enhances spreading. Comparison of nano-droplet impact characteristics under standardized conditions on gold and silicon substrates shows that wettability, as well as heat transfer to the solid substrate, are both important in controlling the initial spread and as well as the subsequent solidification morphology. Simulations combined with experiments show that a high droplet-substrate heat transfer rate, together with high substrate wettability, facilitates spreading and results in a thinner solidified metal deposit.

Funding. National Natural Science Foundation of China (NSFC) (51520105007, 51775299); National Key Research and Development Program of China (2017YFB1104900).

Acknowledgment. The authors thank Dr. Xin Wu for helpful discussions on the MD method.

REFERENCES

1. M. Zenou, A. Sa'ar, and Z. Kotler, "Laser transfer of metals and metal alloys for digital microfabrication of 3D objects," Small **11**, 4082–4089 (2015).
2. C. W. Visser, R. Pohl, C. Sun, G. W. Romer, B. Huis in 't Veld, and D. Lohse, "Toward 3D printing of pure metals by laser-induced forward transfer," Adv. Mater. **27**, 4087–4092 (2015).
3. M. Zenou, A. Sa'ar, and Z. Kotler, "Laser jetting of femto-liter metal droplets for high resolution 3D printed structures," Sci. Rep. **5**, 17265 (2015).

4. U. Zywietz, M. K. Schmidt, A. B. Evlyukhin, C. Reinhardt, J. Aizpurua, and B. N. Chichkov, "Electromagnetic resonances of silicon nanoparticle dimers in the visible," ACS Photon. **2**, 913–920 (2015).
5. U. Zywietz, A. B. Evlyukhin, C. Reinhardt, and B. N. Chichkov, "Laser printing of silicon nanoparticles with resonant optical electric and magnetic responses," Nat. Commun. **5**, 3402 (2014).
6. U. Zywietz, C. Reinhardt, A. B. Evlyukhin, T. Birr, and B. N. Chichkov, "Generation and patterning of Si nanoparticles by femtosecond laser pulses," Appl. Phys. A **114**, 45–50 (2013).
7. A. B. Evlyukhin, S. M. Novikov, U. Zywietz, R. L. Eriksen, C. Reinhardt, S. I. Bozhevolnyi, and B. N. Chichkov, "Demonstration of magnetic dipole resonances of dielectric nanospheres in the visible region," Nano Lett. **12**, 3749–3755 (2012).
8. A. I. Kuznetsov, A. B. Evlyukhin, M. R. Gonçalves, C. Reinhardt, A. Koroleva, M. L. Arnedillo, R. Kiyan, O. Marti, and B. N. Chichkov, "Laser fabrication of large-scale nanoparticle arrays for sensing applications," ACS Nano **5**, 4843–4849 (2011).
9. R. Ganeev, U. Chakravarty, P. Naik, H. Srivastava, C. Mukherjee, M. Tiwari, R. Nandedkar, and P. Gupta, "Pulsed laser deposition of metal films and nanoparticles in vacuum using subnanosecond laser pulses," Appl. Opt. **46**, 1205–1210 (2007).
10. E. Millon, J. Perrière, R. Defourneau, D. Defourneau, O. Albert, and J. Etchepare, "Femtosecond pulsed-laser deposition of $BaTiO_3$," Appl. Phys. A **77**, 73–80 (2003).
11. G. Riboux and J. M. Gordillo, "Experiments of drops impacting a smooth solid surface: a model of the critical impact speed for drop splashing," Phys. Rev. Lett. **113**, 024507 (2014).
12. V. Vaikuntanathan and D. Sivakumar, "Maximum spreading of liquid drops impacting on groove-textured surfaces: effect of surface texture," Langmuir **32**, 2399–2409 (2016).
13. C. Duez, C. Ybert, C. Clanet, and L. Bocquet, "Making a splash with water repellency," Nat. Phys. **3**, 180–183 (2007).
14. P. Tsai, R. C. A. van der Veen, M. van de Raa, and D. Lohse, "How micropatterns and air pressure affect splashing on surfaces," Langmuir **26**, 16090–16095 (2010).
15. L. Xu, W. W. Zhang, and S. R. Nagel, "Drop splashing on a dry smooth surface," Phys. Rev. Lett. **94**, 184505 (2005).
16. A. Latka, A. Strandburg-Peshkin, M. M. Driscoll, C. S. Stevens, and S. R. Nagel, "Creation of prompt and thin-sheet splashing by varying surface roughness or increasing air pressure," Phys. Rev. Lett. **109**, 054501 (2012).
17. D. Shen, G. Zou, L. Liu, W. W. Duley, and Y. N. Zhou, "Investigation of splashing phenomena during the impact of molten sub-micron gold droplets on solid surfaces," Soft Matter **12**, 295–301 (2016).
18. S. D. Aziz and S. Chandra, "Impact, recoil and splashing of molten metal droplets," Int. J. Heat Mass Transfer **43**, 2841–2857 (2000).
19. X.-H. Li, X.-X. Zhang, and M. Chen, "Estimation of viscous dissipation in nanodroplet impact and spreading," Phys. Fluids **27**, 052007 (2015).
20. J. Koplik and R. Zhang, "Nanodrop impact on solid surfaces," Phys. Fluids **25**, 022003 (2013).
21. P. J. Rossky, "Exploring nanoscale hydrophobic hydration," Faraday Discuss. **146**, 13–18 (2010).
22. G. He and N. G. Hadjiconstantinou, "A molecular view of Tanner's law: molecular dynamics simulations of droplet spreading," J. Fluid Mech. **497**, 123–132 (2003).
23. M. S. Daw and M. I. Baskes, "Semiempirical, quantum mechanical calculation of hydrogen embrittlement in metals," Phys. Rev. Lett. **50**, 1285–1288 (1983).
24. S. R. Billeter, A. Curioni, D. Fischer, and W. Andreoni, "Ab initio derived augmented Tersoff potential for silicon oxynitride compounds and their interfaces with silicon," Phys. Rev. B **73**, 155329 (2006).
25. J. Tersoff, "Modeling solid-state chemistry: interatomic potentials for multicomponent systems," Phys. Rev. B **39**, 5566–5568 (1989).
26. J. Tersoff, "Empirical interatomic potential for silicon with improved elastic properties," Phys. Rev. B **38**, 9902–9905 (1988).
27. J. L. Barrat, "Large slip effect at a nonwetting fluid-solid interface," Phys. Rev. Lett. **82**, 4671–4674 (1999).
28. G. Hummer and S. Garde, "Cavity expulsion and weak dewetting of hydrophobic solutions in water," Phys. Rev. Lett. **80**, 4193–4196 (1998).
29. Q. Pu, Y. Leng, X. Zhao, and P. T. Cummings, "Molecular simulations of stretching gold nanowires in solvents," Nanotechnology **18**, 424007 (2007).
30. F. H. Stillinger and T. A. Weber, "Computer simulation of local order in condensed phases of silicon," Phys. Rev. B **31**, 5262–5271 (1985).
31. S. Plimpton, "Fast parallel algorithms for short-range molecular dynamics," J. Comput. Phys. **117**, 1–19 (1995).
32. P. H. Hünenberger, "Thermostat algorithms for molecular dynamics simulations," in *Advanced Computer Simulation* (Springer, 2005), pp. 105–149.
33. C. M. Muller, F. C. Mornaghini, and R. Spolenak, "Ordered arrays of faceted gold nanoparticles obtained by dewetting and nanosphere lithography," Nanotechnology **19**, 485306 (2008).
34. B. Ressel, K. C. Prince, S. Heun, and Y. Homma, "Wetting of Si surfaces by Au-Si liquid alloys," J. Appl. Phys. **93**, 3886–3892 (2003).
35. J. T. Hirvi and T. A. Pakkanen, "Nanodroplet impact and sliding on structured polymer surfaces," Surf. Sci. **602**, 1810–1818 (2008).